Exact Solutions for the Intrinsic Geometry of Black Hole Coalescence

Luis Lehner[1*], Nigel T. Bishop[2], Roberto Gómez[1],
Bela Szilagyi[1] and Jeffrey Winicour[1]
[1]*Department of Physics and Astronomy,*
University of Pittsburgh, Pittsburgh, PA 15260
[2]*Department of Mathematics, Applied Mathematics and Astronomy,*
University of South Africa, P.O. Box 392, Pretoria 0003, South Africa

Abstract

We describe the null geometry of a multiple black hole event horizon in terms of a conformal rescaling of a flat space null hypersurface. For the prolate spheroidal case, we show that the method reproduces the pair-of-pants shaped horizon found in the numerical simulation of the head-on-collision of black holes. For the oblate case, it reproduces the initially toroidal event horizon found in the numerical simulation of collapse of a rotating cluster. The analytic nature of the approach makes further conclusions possible, such as a bearing on the hoop conjecture. From a time reversed point of view, the approach yields a description of the past event horizon of a fissioning white hole, which can be used as null data for the characteristic evolution of the exterior space-time.

04.20Ex, 04.25Dm, 04.25Nx, 04.70Bw

*Present Address: Center for Relativity, The University of Texas at Austin, Austin TX 78712.

I. INTRODUCTION

Numerical simulations of axisymmetric space-times have enabled construction of the event horizon traced out by the evolution of dynamical black holes [1–6]. Besides confirming behavior dictated by the general laws of black hole dynamics [7,8], the simulations supply further insight which was not anticipated from analytic theory. In the case of a head-on collision, they supply the details of how the holes form and merge [9]. In the case of rotating collapse, they reveal how an initially toroidal structure is compatible with topological censorship [10]. In this paper, we present a 3-dimensional analytic description of the event horizon for a multiple black hole space-time which, in the axisymmetric case, reproduces the qualitative features of the above simulations.

As a stand-alone item, a black hole horizon is a null hypersurface whose cross-sectional surface area monotonically increases and approaches a finite limit in the future. The *number* of black holes contained at a given time is not conventionally defined in terms of such a stand-alone picture but rather in terms of the number of disjoint sections given by the intersection of the horizon with a Cauchy hypersurface [7,8]. In the approach we present here, in the case of the head-on-collision the notion of "two holes" arises intrinsically from a preferred slicing of the horizon based upon an affine parameter along its generating null rays.

For this purpose, we consider the geometry of a null hypersurface $\mathcal{N}$ whose surface area has a finite asymptotic limit. The intrinsic and extrinsic geometrical properties of a null hypersurface cannot be described in terms of the same "3+1" formalism used for a space-like hypersurface. In particular, the degenerate 3-metric of a null hypersurface does not define an intrinsic covariant derivative, in contrast to the case of a space-like hypersurface. Dautcourt [11] has presented an alternative formalism for inducing an intrinsic geometry on a null hypersurface from the embedding geometry. Geroch [12] used a similar approach to describe null infinity $\mathcal{I}$ as a 3-dimensional null hypersurface detached from the physical space-time M. In Sec. II, we take an analogous approach to treat the null hypersurface traced out by a black hole as a stand-alone geometric object.

Numerical investigations [1–6] of event horizons have used the Cauchy initial value problem to evolve a black hole space-time throughout a domain of sufficient extent (both in space and time) so as to include an apparent horizon which has become approximately (but not exactly) stationary. This implies that the marginally trapped surfaces defining the apparent horizon have almost stopped growing in surface area. The event horizon is then located by examining the null geodesics which pass in the vicinity of the last quasi-stationary marginally trapped surface obtained in the evolution. The approach adopted in this paper is rather different. We have developed a method that constructs a null hypersurface whose surface area has finite asymptotic limit and whose intrinsic geometry satisfies all other requirements for a non singular event horizon. Thus, from all intrinsic criteria, this null hypersurface represents an event horizon $\mathcal{H}$. The results of this paper depend only upon the intrinsic geometry of $\mathcal{H}$ and not upon the properties of the embedding space-time (which will be presented in subsequent papers). Even so, in order to show that the results of this paper are physically meaningful, it is necessary to discuss whether there exists a space-time in which $\mathcal{H}$ can be embedded.

There is a formal construction of a vacuum space-time based upon the characteristic initial value problem posed on an intersecting pair of null hypersurfaces [13–15]. Here we

consider two null hypersurfaces intersecting in a topologically spherical surface S_0. Intrinsic geometrical data must be given on the two null hypersurfaces, as well as a quantity, called the twist [14,15], which is analogous to an extrinsic curvature in the Cauchy problem. We can apply this formalism to the case where S_0 is a cross-section of the event horizon at a late quasi-stationary time. Then, referring to Fig. 1, $\mathcal{H}$ intersects the ingoing null hypersurface J^+ at S_0. Characteristic data given on the portion of $\mathcal{H}$ and J^+ to the past of S_0, leads to a formal solution of the vacuum equations in the domain of dependence D^- to the past of S_0. To the extent that S_0 lies in the late time stationary region of the horizon, J^+ approximates future null infinity. So, for a horizon describing a binary black hole, the physically appropriate characteristic data on J^+ would describe the outgoing radiation emitted during the merger, although any data satisfying the constraints would formally lead to a consistent vacuum space-time. (As in the Cauchy problem, Einstein's equations imply constraints on the characteristic initial data but these reduce to propagation equations along the null geodesics so that it is simple to isolate the unconstrained free data.)

There are theorems establishing the existence of solutions to this double null initial value problem [16–18]. Although global issues remain unresolved, these theorems guarantee existence in some neighborhood of the initial hypersurfaces. The double null version of the characteristic initial value problem is equivalent to the world tube - null cone problem [19] in the case where the world tube is null. There exists a stable, accurate and efficient characteristic evolution code [20,21] (the PITT code) which evolves this initial value problem and which could be applied to construct a numerical solution to the situation described in Fig. 1. This provides the local existence of a space-time satisfying Einstein's equations in the finite difference approximation. Ideally, we would like to construct a numerical solution throughout the domain of dependence D^- but that is more problematical. The evolution algorithm requires the foliation of D^- by a one parameter family of null hypersurfaces J_v. However, referring to Fig. 1, such a foliation becomes singular at J_M in the portion of the horizon corresponding to black hole merger. Thus one could only obtain the post-merger space-time by this procedure. This problem is due to a coordinate singularity, not a physical singularity, and from a mathematical point-of-view the space-time is extendable to earlier times; but just how much earlier cannot be answered by a characteristic evolution. Thus the analytic event horizon for a black hole collision, which we present in this paper, can be used as characteristic initial data to construct a vacuum space-time (either analytically or numerically) covering some domain preceding the merger.

A major motivation for the present study stems from a potential indirect application of the results to a calculation of the gravitational waveform radiated by coalescing black holes using the PITT code. Waveforms from highly nonlinear, highly distorted single black holes have already been obtained with this code [20,21]. In these simulations [20], the two null hypersurfaces were chosen to be (i) a portion of the past horizon (white hole) of a Schwarzschild space-time and (ii) an outgoing null hypersurface emanating from a slice of the past horizon to $\mathcal{I}^+$, which (in order to introduce distortion) contains incoming radiation. The code has equal capability of carrying out such simulations with the static Schwarzschild white hole replaced by a dynamic past horizon corresponding to a white hole which is initially stationary and later fissions into a pair of white holes. In a time-reversed scenario, the outgoing waveform from this white hole explosion corresponds to the *incoming* radiation incident from past null infinity on the merger of a pair of black holes. While this is not the

correct physical prescription of initial conditions for black hole coalescence, if the system were linear this incoming radiation could be used to draw inferences about the *outgoing* radiation. Such linearity is of course not expected. Yet any means of obtaining a handle on the merger waveform is of current importance. In addition, a solution of this problem would unambiguously yield the outgoing radiation from a white hole explosion, a system of at least academic interest.

The time reversal of the intrinsic geometry of the event horizon of a black hole, results in the event horizon of a white hole, and vice-versa. The construction developed in this paper is naturally expressed in terms of a white hole that bifurcates in the future, and thus our method is presented for the case of a white hole. The reinterpretation of our results, in terms of a black hole horizon, is straightforward. Thus we pose our investigation in terms of a white hole horizon $\mathcal{H}$, which constitutes a portion of a null hypersurface $\mathcal{N}$, with the property that its surface area decreases into the future and has a a finite asymptotic limit in the past. The null rays of $\mathcal{N}$ leave $\mathcal{H}$ at points where they meet other null rays of $\mathcal{N}$. Such endpoints can occur at a "crossover" point, where initially non-neighboring rays intersect, or at a caustic, where neighboring rays intersect. These properties follow from the fundamental theorems of black hole physics. [7,8]

Note that a crossover point may also be a caustic, as in the case of a spherically symmetric light cone and also in the case of the prolate spheroidal light cone considered in Section IV. In addition, a portion of $\mathcal{N}$ can continue smoothly across a non-caustic crossover point, as in the example of the oblate spheroidal light cone considered in Section IV. However, $\mathcal{H}$ must end at such a crossover point.

In this paper, we do not calculate the gravitational radiation emitted by the system but study only the internal dynamics of $\mathcal{H}$. In Sec. IV we specialize to the axisymmetric case which facilitates an analytic treatment of the endpoints of $\mathcal{H}$. We find that the bifurcation of $\mathcal{H}$ in a white hole explosion has the same "pair-of-pants" structure (in a time reversed sense) observed in the numerical simulation of a head-on collision of black holes. Further features emerge, such as the ultimate fate of an "eternal" pants leg, the details of toroidal black hole formation in the vacuum case and a bearing on a strict version of the hoop conjecture [22].

II. 3-DIMENSIONAL AFFINE NULL GEOMETRY

It is useful to consider $\mathcal{N}$ as one of the null hypersurfaces in the double null initial value problem for the vacuum Einstein equations. As first shown by Sachs [13], the evolution of the double null problem requires as boundary data the intrinsic conformal geometry on $\mathcal{N}$, i.e. a metric γ_{ab} expressed in terms of an affine parameter u, up to the conformal freedom $\gamma_{ab} \rightarrow \Omega^2\gamma_{ab}$. In addition, the intrinsic conformal geometry must be specified on a null hypersurface meeting $\mathcal{N}$ transversely at some cross-section $\mathcal{S}_0$, as well as the intrinsic 2-geometry and certain extrinsic curvature quantities of $\mathcal{S}_0$. Here we restrict our attention to the intrinsic properties of $\mathcal{N}$ and $\mathcal{S}_0$. As emphasized by Hayward [14,15], it is important to consider specification of an affine parameter u on $\mathcal{N}$ as part of the data.

This intrinsic data obey the Sachs equations [23] governing the expansion or contraction of $\mathcal{N}$. As a consequence, the data determine a unique metric γ_{ab} from the conformal equivalence class on $\mathcal{N}$. Here γ_{ab} satisfies the degeneracy condition $\gamma_{ab}n^b = 0$, where n^b is tangent

to the generators of $\mathcal{N}$. We choose n^a to have the affine normalization $n^a\partial_a = \partial_u$.

Our aim is to use a special choice of $\mathcal{N}$ as a stand-alone model of a white hole horizon $\mathcal{H}$. We require that $\mathcal{H}$ be complete in the past and that its surface area have a finite asymptotic limit as $u \to -\infty$. $\mathcal{H}$ ends in the future at points where its generators intersect, either at a caustic or crossover point.

The Sachs equations can be derived by projecting the relevant components of the 4-dimensional Einstein equation into 3-dimensional form. In doing so, we must deal with the degeneracy of γ_{ab} in representing the counterpart of 4-dimensional covariant derivatives as operators on $\mathcal{N}$. The formalism adopted here makes explicit use of the affine structure of $\mathcal{N}$.

We begin with the four dimensional description of $\mathcal{N}$ as a null hypersurface embedded in a vacuum space-time with metric g_{ab} and covariant derivative ∇_a. On $\mathcal{N}$, the affine tangent to the generators satisfies the geodesic equation $n^b\nabla_b n^a = 0$ and the hypersurface orthogonality condition $n^{[a}\nabla^b n^{c]} = 0$ We make no assumptions about the behavior of n^a off $\mathcal{N}$. We project 4-dimensional tensor fields into $\mathcal{N}$ using the operator

$$P_a^b = \delta_a^b + n_a l^b \tag{2.1}$$

where l^a is the unique outgoing null vector field on $\mathcal{N}$ which is orthogonal to the affine cross-sections and satisfies $l^a n_a = -1$. We can set $l_a = -\nabla_a u$, where u is any smooth extension of the affine parameter to a field in the neighborhood of $\mathcal{N}$.

The projected metric $\gamma_{ab} = P_a^c P_b^d g_{cd}$ is the pullback of the 4-metric g_{ab} to $\mathcal{N}$. When restricted to the 2-surfaces determined by the affine foliation, the projected contravariant metric $\gamma^{ab} = P_c^a P_d^b g^{cd}$ is the (unique) inverse of the pullback of g_{ab}.

We introduce the shorthand notation $\perp T_a^b$ for the projection (to the tangent space of $\mathcal{N}$) of a tensor T_a^b. Thus, $\perp n^a = n^a$ and $\perp l_a = l_a$. In addition, the following useful formula hold on $\mathcal{N}$:

$$0 = \perp n_a \tag{2.2}$$
$$0 = \perp l^a \tag{2.3}$$
$$0 = \perp \mathcal{L}_n l_a \tag{2.4}$$
$$0 = \perp \mathcal{L}_n n_a \tag{2.5}$$
$$0 = \perp \nabla_{[a} n_{b]} \tag{2.6}$$
$$\perp \mathcal{L}_n g_{ab} = \mathcal{L}_n \gamma_{ab} \tag{2.7}$$
$$\perp \mathcal{L}_n^2 g_{ab} = \mathcal{L}_n^2 \gamma_{ab}. \tag{2.8}$$

The last two of these equations can be verified using the commutation relation

$$0 = \perp [\mathcal{L}_n, \perp]. \tag{2.9}$$

Our purpose is to rewrite the projected curvature components $\Phi_{ab} = \perp n^c n^d R_{cabd} = \perp n^c(\nabla_c\nabla_a - \nabla_a\nabla_c)n_b$ in a form intrinsic to $\mathcal{N}$. By applying the above formulae, we obtain

$$\Phi_{ab} = \frac{1}{2}\mathcal{L}_n^2\gamma_{ab} - \frac{1}{4}\gamma^{cd}(\mathcal{L}_n\gamma_{ac})\mathcal{L}_n\gamma_{bd}. \tag{2.10}$$

This further simplifies by setting $\gamma_{ab} = R^2 h_{ab}$ and $\gamma^{ab} = R^{-2} h^{ab}$ where $h^{ab}\mathcal{L}_n h_{ab} = 0$. (This can be achieved by choosing R^2 as the determinant of the restriction of γ_{ab} to the surfaces of the affine foliation.) Then, in terms of the shear tensor $\Sigma_{ab} = \mathcal{L}_n h_{ab}$,

$$\Phi_{ab} = \frac{1}{2}\mathcal{L}_n(R^2 h_{ab}) + h_{ab} R \mathcal{L}_n^2 R - \frac{1}{4} R^2 h^{cd}\Sigma_{ac}\Sigma_{bd}. \tag{2.11}$$

The Sachs equations follow immediately from Eq. (2.11). Taking the trace of Φ_{ab} results in

$$n^c n^d R_{cd} = -\frac{2\mathcal{L}_n^2 R}{R} - \frac{1}{2}\Sigma^2, \tag{2.12}$$

where R_{cd} is the Ricci tensor and where $\Sigma^2 = (1/2)h^{ab}h^{cd}\Sigma_{ac}\Sigma_{bd}$. Then in the *vacuum case* it follows that

$$\mathcal{L}_n^2 R = -\frac{1}{4} R\Sigma^2. \tag{2.13}$$

The trace free part of Eq. (2.11) yields

$$\Psi_{ab} = \frac{1}{2}\mathcal{L}_n(R^2\Sigma_{ab}) - \frac{1}{2}R^2\Sigma^2 h_{ab}. \tag{2.14}$$

where Ψ_{ab} are projected components of Weyl curvature.

We proceed further to decompose the shear in terms of its normalized eigenvectors p^a and q^a satisfying $\Sigma_{ab}(p^b + iq^b) = \Sigma h_{ab}(p^b - iq^b)$. Then $h_{ab} = p_a p_b + q_a q_b$ and $\Sigma_{ab} = \Sigma(p_a p_b - q_a q_b)$, where $p_a + iq_a = h_{ab}(p^b + iq^b)$ and satisfies $p^a\mathcal{L}_n p_a + q^a\mathcal{L}_n q_a = 0$ and $p^a\mathcal{L}_n q_a + q^a\mathcal{L}_n p_a = 0$.

The goal is to solve Eq. (2.13) in a way consistent with a white hole horizon $\mathcal{H}$ on a portion of $\mathcal{N}$. Thus the Weyl curvature must be non-singular on $\mathcal{H}$. This requires that the contraction Ψ_{ab} with a unit vector (normalized with respect to γ_{ab}) yield a non-singular scalar field on $\mathcal{H}$ (including the endpoints of $\mathcal{H}$); i.e. that

$$\Psi = R^{-2}(p^a + iq^a)(p^b + iq^b)\Psi_{ab} = R^{-2}\mathcal{L}_n(R^2\Sigma) + i\Sigma(q^a\mathcal{L}_n p_a - p^a\mathcal{L}_n q_a) \tag{2.15}$$

be non-singular.

III. CONFORMALLY FLAT NULL GEOMETRY

The Weyl smooth solutions of Eq. (2.13) have a large degree of freedom corresponding to the outgoing radiation crossing $\mathcal{N}$. In order to restrict this freedom we consider solutions whose null metric is conformal to that of a null hypersurface embedded in a flat Minkowski space-time.

Consider then the flat space case, where we denote the corresponding fields on $\mathcal{N}$ as $\hat{\gamma}_{ab}$, $\hat{R}$, $\hat{h}_{ab}$, $\hat{n}^a$, $\hat{u}$, etc. For convenience, we write $F' = \mathcal{L}_{\hat{n}}F$ for tensor fields F. Since $\hat{\Psi}_{ab} = 0$, Eq. (2.14) implies $(\hat{p}^a + i\hat{q}^a)(\hat{p}_a - i\hat{q}_a)' = 0$ and $\hat{R}^2\hat{\Sigma} = \sigma$, where $\sigma' = 0$. The conditions on the eigenvectors may be summarized by $\hat{p}'_a = (\Sigma/2)\hat{p}_a$ and $\hat{q}'_a = -(\Sigma/2)\hat{q}_a$.

The focusing equation (2.13) now integrates to give

$$\hat{R}^2 = (A\hat{u} + B)^2 - \frac{1}{4}\sigma^2, \tag{3.1}$$

where $A' = B' = 0$. We adjust the affine freedom in $\hat{u}$ so that $\hat{R} \to \hat{u}$ as $\hat{u} \to \infty$ and so that the two caustics of $\hat{R}$ are placed symmetrically. Then Eq. (3.1) reduces to

$$\hat{R}^2 = (\hat{u} + \frac{1}{2}\sigma)(\hat{u} - \frac{1}{2}\sigma). \tag{3.2}$$

We choose conventions so that the $\sigma \geq 0$, so that the caustic corresponding to the q principle direction is reached first, moving along a ray in the direction of increasing $\hat{u}$.

The dependence of the eigenvectors is determined to be

$$\hat{p}_a = \left(\frac{\hat{u} - \sigma/2}{\hat{u} + \sigma/2}\right)^{1/2} P_a \tag{3.3}$$

$$\hat{q}_a = \left(\frac{\hat{u} + \sigma/2}{\hat{u} - \sigma/2}\right)^{1/2} Q_a \tag{3.4}$$

where $(P_a + iQ_a)' = 0$. The resulting $\hat{u}$-dependent family of 2-metrics, comprise the classic description of the 2-geometries generated by the parallel map [24] of a surface $\mathcal{S}_0$ embedded in Euclidean space. The parallel map consists of translations by the same distance $\Delta\hat{u}$ along each normal to the surface (identical to Huyghen's construction for propagating a wavefront). Equivalently, by considering $\mathcal{S}_0$ to be embedded at time $t = 0$ in a Minkowski space-time, the translation along each ingoing normal null direction through the time $\Delta\hat{u} = t$, generates a null-hypersurface foliated by constant time slices $\hat{S}_t$.

In applying this construction, we choose $\mathcal{S}_0$ to be convex so that $\hat{S}_t$ traces out the flat space wavefronts of a null hypersurface converging in the inward direction. From the point of view of the flat embedding, σ is the distance between the two caustics generically encountered along each null ray.

Given such a flat space null hypersurface, with the convexity property that its caustics are reached at finite $\hat{u}$, we generate a curved space null cone with the same conformal structure, i.e. $\gamma_{ab} = \Omega^2\hat{\gamma}_{ab}$. We thus set $R = \Omega\hat{R}$ and $h_{ab} = \hat{h}_{ab}$. We do not require that the two affine structures agree and set $n^a = \Lambda\hat{n}^a$ so that $\partial_u = \Lambda\partial_{\hat{u}}$ and $\Sigma = \Lambda\hat{\Sigma}$. Our goal is to investigate the properties of the foliation S_t determined by translating $\mathcal{S}_0$ through the curved space affine time $\Delta u = t$.

The curved space focusing equation (2.13) now reduces to

$$\Lambda'(\Omega'\hat{R} + \Omega\hat{R}') + \Lambda(\Omega''\hat{R} + 2\Omega'\hat{R}') = 0; \tag{3.5}$$

and the Weyl curvature, defined in Eq. (2.14), reduces to

$$\Psi_{ab} = \frac{\sigma\Lambda}{2}(\Omega^2\Lambda)'(p_a p_b - q_a q_b) \tag{3.6}$$

with the Weyl scalar, defined in Eq. (2.15), given by

$$\Psi = \sigma\frac{\Lambda(\Omega^2\Lambda)'}{\Omega^2\hat{R}^2}. \tag{3.7}$$

The goal is to solve these equations to construct a non-singular white hole horizon $\mathcal{H}$. Then Ψ must be non-singular on $\mathcal{H}$ and the scalar fields Ω and Λ must be smooth positive functions, except possibly at the endpoints of $\mathcal{H}$. In addition, the surface area of $\mathcal{H}$ must approach a finite limit as $u \to -\infty$.

We require that u and $\hat{u}$ approach $-\infty$ together at the same rate so that we may restrict the affine freedom in u by requiring that $u' \to 1$. The surface area function must have a finite limit $R \to R_\infty$ as $u \to -\infty$, corresponding to an irreducible mass [8] $M_\infty = R_\infty/2$. Then, from inspection of Eq. (3.7), $\Omega\hat{u} \to -R_\infty$ and $\Lambda \to 1$, as $\hat{u} \to -\infty$. We also assume that these conditions are uniformly satisfied along each null ray in terms of a $1/\hat{u}$ expansion. This puts constraints on the fields Λ and Ω which satisfy Eq. (3.5). In order to apply these conditions it is convenient to introduce the function $F = \Lambda\Omega^2$. Then the smoothness of Ψ requires that $F' = 0$ at a caustic. Also, the asymptotic conditions on Ω and Λ as $\hat{u} \to -\infty$ require $\hat{u}^2 F \to R_\infty^2$ so that, $\hat{u}(logF)' \to -2$.

Equation (3.5) can now be rewritten in terms of F and Ω as

$$(logF)' = \frac{\Omega[1/\Omega]''}{[log(\Omega\hat{R})]'}. \tag{3.8}$$

We can generate solutions to Eq. (3.8) by making an ansatz for Ω and then integrating to determine F. The above smoothness condition that F must satisfy at a caustic is then automatically satisfied if Ω is smooth. The asymptotic conditions require that the ansatz satisfy $\Omega\hat{R} \to R_\infty + O(1/\hat{u}^2)$ and $u^2(\Omega\hat{R} - 1) \to -\sigma^2/24$.

In order for the resulting model to represent a non-singular white hole, additional conditions arise at a shear-free ray. Along such a ray, the focusing equation (2.13) implies that $\partial_u^2 R = 0$ with solution $R = C_1 + C_2 u$. Accordingly, R must be a constant along each ray since it approaches a finite limit R_∞ as $u \to -\infty$. Thus we must require that our ansatz reduce to $\Omega = R_\infty/\hat{R}$ along a shear-free ray. Such rays occur at any umbilical point of $\mathcal{S}_0$ where the two curvature eigenvalues are equal and $\sigma = 0$. For surfaces of revolution the poles are always umbilical. Umbilics are a major factor in determining the qualitative behavior of the white hole model. Along a non-umbilical ray, the completeness of $\mathcal{H}$ as a white hole model requires that the range of u extend to a crossover point or caustic, where it hits another ray and the hole terminates. However, along an umbilic, the white hole need not terminate and can extend to infinite u. As we shall illustrate, this is the mechanism which leads to multiple black holes in a u-foliation of $\mathcal{H}$.

The behavior at umbilics imposes further conditions on our ansatz. For example, suppose that the white hole terminates along a set of non-umbilical caustics $\hat{u} = -\sigma/2$ which has an endless umbilic ray on its boundary where $\sigma = 0$. Then u must be finite along the non-umbilic set but approach ∞ as $\sigma \to 0$. Also, $u' = 1/\Lambda$ must have the same behavior since the caustic set, including its boundary, is reached at finite $\hat{u}$.

The simple ansatz

$$\Omega = -R_\infty(\hat{u} + \frac{\sigma^2}{12(\rho - \hat{u})})^{-1} \tag{3.9}$$

satisfies all the above conditions if the parameter ρ is chosen so that $\rho \geq \sigma/\sqrt{13}$. Then $\Omega > 0$ in the white hole region contained inside $\hat{u} \leq -\sigma/2$. Furthermore, integration of Eq. (3.8) gives

$$F = \frac{16R_\infty^2(\hat{u}-\rho)^2\,(2\hat{u}-5\rho+\mu)^{2\,(2\rho/\mu-1)}}{(2\hat{u}-5\rho-\mu)^{2\,(2\rho/\mu+1)}} \tag{3.10}$$

and

$$u' = \frac{9}{(12\hat{u}(\hat{u}-\rho)-\sigma^2)^2}\frac{(2\hat{u}-5\rho-\mu)^{2\,(2\rho/\mu+1)}}{(2\hat{u}-5\rho+\mu)^{2\,(2\rho/\mu-1)}}\,, \tag{3.11}$$

where $\mu=\sqrt{13\rho^2-\sigma^2}$ is real and positive. The asymptotic expansion of the integral gives

$$u = \hat{u} - 12\,\rho\,\ln\hat{u} + C + O(\frac{1}{\hat{u}}), \tag{3.12}$$

where C is the integration constant.

On the caustic set $\hat{u}=-\sigma/2$, we have

$$\Psi = \frac{8\sigma^4}{81(\sigma+2\rho)^6(\sigma+3\rho)}\left(\frac{\sigma+5\rho-\mu}{\sigma+5\rho+\mu}\right)^{8\rho/\mu}\,, \tag{3.13}$$

which is manifestly regular; and

$$u' = \frac{9(\sigma+2\rho)^2}{\sigma^2}\left(\frac{\sigma+5\rho+\mu}{\sigma+5\rho-\mu}\right)^{4\rho/\mu}\,, \tag{3.14}$$

which displays the required singular behavior as $\sigma\to 0$ at an umbilical point and is otherwise regular.

It is instructive to examine the behavior of the extrinsic curvature eigenvalues defined on $\mathcal{H}$ according to

$$\kappa_p = \frac{p^a p^b \mathcal{L}_n\gamma_{ab}}{2R^2} = \frac{\Sigma}{2} + \frac{\partial_u R}{R} \tag{3.15}$$

and

$$\kappa_q = \frac{q^a q^b \mathcal{L}_n\gamma_{ab}}{2R^2} = -\frac{\Sigma}{2} + \frac{\partial_u R}{R}. \tag{3.16}$$

For our flat space model, $\hat{\kappa}_p = 1/(\hat{u}-\sigma/2)$ and $\hat{\kappa}_q = 1/(\hat{u}+\sigma/2)$. Then $\kappa_{(p,q)} = \Lambda(\hat{\kappa}_{(p,q)} + \Omega^{-1}\partial_{\hat{u}}\Omega)$. For the ansatz (3.9), these reduce to

$$\kappa_p = \frac{\sigma(12u(u-\rho)-\sigma^2)(12(u-\rho)^2+\sigma(\sigma-4u+2\rho))}{9(u-\rho)(2u-\sigma)}\frac{(-2u+5\rho-\mu)^{2[(2\rho/\mu)-1]}}{(-2u+5\rho+\mu)^{2[(2\rho/\mu)+1]}} \tag{3.17}$$

and

$$\kappa_q = \frac{-\sigma(12u(u-\rho)-\sigma^2)(12(u-\rho)^2+\sigma(\sigma+4u-2\rho))}{9(u-\rho)(2u+\sigma)}\frac{(-2u+5\rho-\mu)^{2[(2\rho/\mu)-1]}}{(-2u+5\rho+\mu)^{2[(2\rho/\mu)+1]}}. \tag{3.18}$$

Both κ_p and κ_q approach 0 as the white hole approaches "equilibrium" as $u\to-\infty$. However, for large negative u it is clear from examining the dominant terms in Eq's (3.17) and (3.18) that $\kappa_p>0$ and $\kappa_q<0$. So, although the mean curvature of $\mathcal{H}$ is negative in agreement with net focusing, $\mathcal{H}$ expands in the p principle direction. As illustrated in Sec. IV, the effect of this expansion as it becomes stronger near the q-caustic provides the characteristic shape of a bifurcating horizon.

IV. THE CONFORMALLY SPHEROIDAL CASE

The preceding analysis describes the dependence of the null geometry of $\mathcal{H}$ on affine parameter along a ray. In order to obtain a model of an exploding white hole we examine the global dependence of the geometry on the angular coordinates parameterizing the rays of $\mathcal{H}$. In the simplest case, $\mathcal{S}_0$ is a sphere. Then $\sigma = 0$ on all rays, $\hat{h}_{ab} = q_{ab}$ the unit sphere metric, $\hat{R} = -\hat{u}$ and the ansatz Eq.(3.9) reduces to $R = R_\infty$ so that the horizon is stationary. A conformally spherical white (black) hole is topless (bottomless) along all rays.

Since all topologically spherical geometries are conformally related, the conformal null geometry of a stationary white (or black) hole is unique. What distinguishes a Kerr horizon from a Schwarzschild horizon is the initial geometry of $\mathcal{S}_0$, which determines R_∞. In the Kerr case, R_∞ is the conformal factor relating the geometry of the Kerr horizon to the unit sphere. (The spin of the Kerr hole arises from an extrinsic geometric quantity which can also be freely specified on $\mathcal{S}_0$). In the Schwarzschild case, R_∞ can chosen to be a constant (independent of angle).

In the case in which $\mathcal{S}_0$ is a prolate spheroid (ellipsoid of revolution), we will show how the identical horizon structure arises, as found in the simulation of colliding black holes. Furthermore, in the oblate case, we will show how a temporarily toroidal horizon arises, as found in the simulation of rotating collapse.

We start with the 2-dimensional surface $\mathcal{S}_0$ describing the spheroid

$$\frac{x^2+y^2}{a^2} + \frac{z^2}{b^2} = 1\,, \tag{4.1}$$

which can be alternatively described in coordinates $y^A = (\theta, \phi)$, by the map

$$x = a\sin\theta\cos\phi \tag{4.2}$$
$$y = a\sin\theta\sin\phi \tag{4.3}$$
$$z = b\cos\theta\,, \tag{4.4}$$

with $\theta \in [0,\pi]$ and $\phi \in [0, 2\pi)$. The intrinsic metric of $\mathcal{S}_0$ is

$$\hat{g}_{AB}dy^A dy^B = (a^2\cos^2\theta + b^2\sin^2\theta)d\theta^2 + a^2\sin^2\theta d\phi^2\,. \tag{4.5}$$

The determinant condition provides a way to define $\hat{R}^2$ as

$$\hat{R}^2 = \frac{det(\hat{g})}{det(q)}, \tag{4.6}$$

(with q_{AB} the unit sphere metric in (θ,ϕ) coordinates). Therefore, $\hat{R}^2 = a\sqrt{b^2\sin^2\theta + a^2\cos^2\theta}$. A straightforward calculation provides the principal radii of curvature of $\mathcal{S}_0$,

$$r_\theta = \frac{(a^2\cos^2\theta + b^2\sin^2\theta)^{3/2}}{ab} \tag{4.7}$$

and

$$r_\phi = \frac{a\sqrt{a^2\cos^2\theta + b^2\sin^2\theta}}{b}\,. \tag{4.8}$$

We consider $\mathcal{S}_0$ to be isometrically embedded at time $t = 0$ in Minkowski space and identify the $\hat{u}$ foliation of $\mathcal{H}$ with the (ingoing) null hypersurface emanating from $\mathcal{S}_0$. We invariantly identify the function σ in our model of $\mathcal{H}$ as the difference between the principle curvatures of $\mathcal{S}_0$:

$$\sigma = |r_\theta - r_\phi| = \frac{|b^2 - a^2|\sin^2\theta\sqrt{a^2\cos^2\theta + b^2\sin^2\theta}}{ab}. \tag{4.9}$$

We set $\hat{u} = u_0$ on $\mathcal{S}_0$. Then our convention that $\hat{u} = 0$ midway between the two caustics of $\mathcal{H}$ allows us to invariantly identify

$$u_0 = -\frac{(r_\theta + r_\phi)}{2} = -\frac{(2a^2 + (b^2 - a^2)\sin^2\theta)\sqrt{a^2\cos^2\theta + b^2\sin^2\theta}}{2ab}. \tag{4.10}$$

This determines both the metric $\hat{\gamma}_{ab}$ and affine parameter $\hat{u}$ for the flat spheroidal null cone.

The conformal factor for the metric $\gamma_{ab} = \Omega^2\hat{\gamma}_{ab}$ of the curved space version is determined by the ansatz Eq.(3.9). Here, in order to satisfy smoothness conditions, we require that the parameter $\rho \geq \sigma_M/\sqrt{13}$, where σ_M is the maximum value of σ attained on $\mathcal{S}_0$. For $a \leq b\sqrt{3}$, the maximum occurs at the equator and $\sigma_M = |b^2 - a^2|/a$. For the highly oblate case with $a > b\sqrt{3}$, the maximum occurs between the equator and poles and $\sigma_M = 2a^2/(3\sqrt{3}b)$.

To determine the curved space affine parameter, we set $u = u_0$ on $\mathcal{S}_0$. Along with the condition that $\partial u/\partial\hat{u} \to 1$ as $\hat{u} \to -\infty$ this fixes the remaining affine freedom in u, i.e. the ray dependent integration constant C in Eq. (3.12). With this choice, $u = \hat{u}$ on $\mathcal{S}_0$ and $\partial_u/\partial_{\hat{u}} \to 1$ as $\hat{u} \to -\infty$.

Figure 2 illustrates the features of the flat space spheroidal null hypersurface $\mathcal{N}_{flat}$, with horizontal lines corresponding to the foliation $\hat{S}_t$ given by $\hat{u} = u_0 + t$. In the illustration, we suppress the rotational symmetry. As discussed below, when the spheroid is prolate (oblate), the crossover points X where $\mathcal{N}_{flat}$ pinches off is a space-like line (disc). The features of the conformally related curved space version $\mathcal{N}$ are quite similar when viewed with respect to the Minkowski foliation $\hat{S}_t$. The chief difference is the effect of the conformal factor on the expansion and shape of the surfaces $\hat{S}_t$, which produces a finite surface area as $\hat{u} \to -\infty$. The features of $\mathcal{N}$ with respect to the curved space affine foliation S_t, given by $u = u_0 + t$, are qualitatively similar to those for $\hat{S}_t$ at early times. The interesting black hole physics occurs near the crossover region of where the foliations S_t and $\hat{S}_t$ have topologically different properties. These are best illustrated by embedding techniques.

A. Embedding

Embedding diagrams constitute valuable tools for visualizing the intrinsic geometry of a curved 2-dimensional surface. By embedding the surface in a flat 3-dimensional Euclidean space, one obtains a surface with the same intrinsic geometry. The following technique was developed by Smarr, who applied it to the description of the Kerr black hole [25]. More

recently, it has been employed to analyze the event horizon of the head-on-collision of black holes [26]. Here we describe its application to our model.

The first step is to introduce the angular coordinate $\eta = \cos\theta$ which makes $det(q_{AB}) = 1$. In $(\hat{u}, \eta, \phi)$ coordinates, the intrinsic metric of the horizon is

$$\gamma_{ab} dx^a dx^b = \Omega^2 \hat{R}^2 (f^{-1} d\eta^2 + f d\phi^2) \tag{4.11}$$

where

$$f = \frac{(1-\eta^2)(\hat{u}+\sigma/2)}{(\hat{u}-\sigma/2)}. \tag{4.12}$$

This can then be transformed into (u, η, ϕ) coordinates by the substitution $\hat{u} = \hat{u}(u, \eta, \phi)$, where $\hat{u}(u, \eta, \phi)$ is determined by integrating Eq. (3.11). The results of this paper are based upon carrying out the integral by means of a Taylor expansion in u about u_0 up to 6th order. (No substantial change in our results were seen in going from 4th order to 6th).

Now, one can isometrically embed this surface in a 3-dimensional Euclidean space with Cartesian coordinates x^i by the map

$$x^1 = F(\eta)\cos\phi,\ x^2 = F(\eta)\sin\phi,\ x^3 = G(\eta), \tag{4.13}$$

where

$$\begin{aligned} F &= \Omega\hat{R}\sqrt{f} \\ G_{,\eta} &= \sqrt{\Omega^2\hat{R}^2/f - F_{,\eta}^2}. \end{aligned} \tag{4.14}$$

The quantities F and G are used to display the surface in the familiar 3-dimensional flat space at a given instant of time determined by the u foliation. Moreover, one can monitor the embedding at different instants of time and produce an "embedding history" which shows the evolution of the surface's geometry. By suppressing the ϕ direction one can stack $\phi = const$ cross-sections of the embedding of the S_t foliation in a three-dimensional fashion, with the vertical axis labeling t and the horizontal axes labeling $F = \sqrt{(x^1)^2 + (x^2)^2}$ and $G = x^3$.

B. The pair-of-pants

We first describe the prolate case $b > a$ in which the crossover points X in the flat-space model are also a line of caustics with respect to the ϕ principle direction. (Thus the ϕ direction corresponds to the q principle direction). In Fig. 2 the rotational symmetry has been factored out so a Minkowski time foliation $\hat{S}_t$ of the underlying flat space spheroidal null hypersurface corresponds to horizontal lines. The effect of curvature focuses the conformally related null hypersurface $\mathcal{N}$ and introduces an upward bulge in the S_t foliation, which gets enhanced at later times to produce the slice S^* at which the white hole bifurcates. The vertical time sequence in our figures corresponds to white holes but the figures can be turned upside-down to depict the corresponding scenario for black holes, in this case a black

hole merger. The points C represent the caustics at the poles which are reached at finite times in the flat model but correspond to infinite affine times in the curved model.

Profiles of the embedding diagram of S_t at various stages are shown in Fig. 3. Proceeding backward in time from the initial prolate spheroid $\mathcal{S}_0$, the cross-sections form the sphere S_{inf} as $t \to -\infty$. Proceeding forward in time, they form the surface S^* (also indicated in Fig. 2) where the white hole is at the verge of fissioning. Note that the two white holes which are produced each have a sharp point at their inner pole.

Fig. 4 shows a time stacking of embedding diagrams of the S_t foliation to form an (inverted) pair-of-pants and Fig. 5 gives a cutaway view of the bifurcation. The main features of the pair-of pants agree with those found in numerical simulation of the head-on vacuum black hole collision [2], as described in Ref's [9,26]. However, the analytic nature of the present work allows us to draw the following further conclusions. First, for the vacuum case, the pair-of-pants is eternal along the two umbilical rays at the poles. However, the legs pinch off and shrink asymptotically since every other ray eventually reaches the crossover X at finite u. Also, referring to the discussion following Eq. (3.18), the principle curvature κ_q corresponding to the θ direction is everywhere negative, except at the poles and in the limit $\hat{u} \to -\infty$ where $\kappa_q = 0$. It is most negative along the equatorial rays, which gives rise to the bow-legged shape of the pair-of-pants.

C. Toroidal horizons and the hoop conjecture

In the oblate case $a > b$, the crossover points X in Fig. 2 (in which the orbits of the rotational symmetry have been factored out) correspond to the same crossover points as in the prolate case. The difference between the two cases is the orientation of the axis of rotation. Whereas X lies on the rotation axis in the prolate case (and thus determines a caustic line under revolution), in the oblate case X rotates to form a disc. Only the outer rim of the disc (generated by revolution of the equatorial points C in Fig. 2) consists of caustic points.

Note that the induced metric $\gamma_{ab}|_X$ of the crossover disc is single-valued (except at the caustic rim C where it is singular); i.e, its value does not depend upon whether X is approached from the top or bottom. This is because (i) by construction of $\mathcal{N}$ as a null hypersurface embedded in Minkowski space, $\hat{\gamma}_{ab}|_X$ is single-valued and (ii) the conformal factor Ω has reflection symmetry with respect to the equatorial plane. More generally, in the absence of symmetry, establishment of consistency conditions for a single-valued metric on the crossover surface would be more complicated.

In the oblate case the θ direction has the smallest radius of curvature (corresponding to the q principle direction). The umbilical rays at the poles cross before they caustic, so that the infinite umbilical stretch in the S_t foliation for the prolate case does not arise in the oblate case. Thus the event horizon is completed in finite affine time, in contrast to the prolate case.

Another important difference also arises in this case. The umbilical stretch produces toroidal cross-sections of the horizon, rather than the two spherical sections arising in the prolate case. The details of the formation of the torus are best understood in terms of the affine displacement $\Delta u(\theta)$ between $\mathcal{S}_0$ and X, as a function of the θ-coordinate of the ray.

In terms of Minkowski time, the corresponding time displacement is [10]

$$\Delta\hat{u}(\theta) = b^2\sqrt{\frac{\sin^2\theta}{a^2} + \frac{\cos^2\theta}{b^2}}\,. \tag{4.15}$$

Then

$$\Delta u(\theta) = \int_{u_0}^{u_0+\Delta\hat{u}} u' d\hat{u}\,, \tag{4.16}$$

where u' is given by Eq. (3.11) and u_0 by Eq. (4.10). In the oblate case, $\Delta\hat{u}$ has its minima at the equator but Δu has minima at the poles and exhibits a monotonic growth towards the equator. As a result, the S_t foliation first touches X at the space-time point where the two polar rays intersect, creating a surface of revolution with the same double teardrop profile as S^* in Fig. 3, but now rotated about the vertical axis through the center. In successive cross-sections, S_t forms a torus (with sharp inner rim), which shrinks to a circle as the horizon terminates. The tidal deformation introduced in the S_t foliation of the curved space model is somewhat analogous to the pair-of-pants shape, except now the identifications of the suppressed rotational symmetry lead to a toroidal topology of S_t for a period of time following the bifurcation. This regime corresponds to the scenario found in the numerical simulation of the collapse of a rotating cluster of particles [1,3,10].

Euclidean embedding is not possible for this full sequence of toroidal white hole formation. Similar results were previously noted by Smarr [25] in regard to the non-existence of a Euclidean embedding for high angular momentum Kerr black holes. The schematic profiles in Fig. 6 indicate the qualitative topological features of the evolution.

The analytic nature of the present approach allows us to draw further conclusions. In the oblate case, the p principle curvature direction in which κ_p is positive corresponds to the ϕ direction, so that the equatorial circumference C is always larger than its asymptotic value $2\pi R_\infty$. This has important bearing on the hoop conjecture [22], which in its original formulation would require that $C \lesssim 4\pi M$. The exact nature of the mass M and of the inequality were purposely left vague in the statement of the conjecture for purposes of further mathematical refinement. If we identify M as the irreducible mass associated with the surface area $4\pi R_\infty^2$ then $M = R_\infty/2$ and $C > 4\pi M$ at every finite u. The largest value of C occurs at the equatorial rim of the crossover disc where

$$C_X = \frac{3(\sqrt{13}+2)}{(\sqrt{13}+3)}[4\pi M] \approx 2.546[4\pi M], \tag{4.17}$$

for the choice $\rho = \sigma_M$ (which maximizes the result). Although our model should not be expected to provide the sharpest bound, this result suggests a significant restriction on any plausible version of the hoop conjecture.

V. CONCLUSION

We have shown that it is possible to treat multiple black or white holes via a stand-alone-model of the event horizon based upon constraint equations for the characteristic

initial value problem. In this paper, we have concentrated on the constraint governing the internal geometry of the horizon. Remarkably, this single equation produces such rich results. Even more interesting features should be expected for models conformal to flat space null hypersurfaces with more structure than the spheroidal case considered here.

In subsequent work, we will extend the treatment to the constraint governing the extrinsic curvature. The boundary conditions provided by the solution of this constraint problem is the missing ingredient necessary to evolve the exterior space-time by means of an existing characteristic code.

ACKNOWLEDGMENTS

This work has been supported by NSF PHY 9510895 and NSF INT 9515257 to the University of Pittsburgh and by the Binary Black Hole Grand Challenge Alliance, NSF PHY/ASC 9318152. N.T.B. thanks the Foundation for Research Development, South Africa, for financial support, and the University of Pittsburgh for hospitality. L.L. thanks the Universities of South Africa and of Durban-Westville for their hospitality. Computer time for the graphical representations was provided by the Pittsburgh Supercomputing Center under grant PHY860023P. We thank Joel Welling of the PSC for assistance with the visualizations. We are especially grateful to Sascha Husa for important discussions and a critical reading of the manuscript.

REFERENCES

[1] S. Shapiro and S. Teukolsky, *Phys. Rev.* **D45**, 2739 (1992).

[2] P. Anninos, D. Hobill, E. Seidel, L. Smarr, and W.-M. Suen, *Phys. Rev. Lett.* **71**, 2851, (1993).

[3] S. A. Hughes, C. R. Keeton, P. Walker, K. Walsh, S. L. Shapiro, and S. A. Teukolsky, *Phys. Rev.* **D49**, 4004 (1994).

[4] A. M. Abrahams, G. B. Cook, S. L. Shapiro, and S. A. Teukolsky, *Phys. Rev. D* **D49**, 5153 (1994).

[5] P. Anninos, D. Bernstein, S. Brandt, J. Libson, J. Massó, E. Seidel, L. Smarr, W.-M. Suen, and P. Walker, *Phys. Rev. Lett.* **74**, 630 (1995).

[6] J. Libson, J. Massó, E. Seidel, L. Smarr, W-M Suen, P. Walker, *Phys. Rev. D***53**, 4335 (1995).

[7] S. W. Hawking, and G. F. R. Ellis, *The Large Scale Structure of Spacetime* (Cambridge University Press, Cambridge, 1973).

[8] R. Wald, *General Relativity* (University of Chicago Press, Chicago, 1984).

[9] R. A. Matzner, H. E. Seidel, S. L. Shapiro, L. Smarr, W-M Suen, S. A. Teukolsky, and J. Winicour, *Science* **270**, 941 (1995).

[10] S. Shapiro, S. Teukolsky and J. Winicour, *Phys. Rev.* **D52**, 6982 (1995).

[11] G. Dautcourt, *J. Math. Phys.* **8**, 1492 (1967).

[12] R. Geroch, in *Asymptotic Structure of Space-Time* (Plenum Press, New York, 1977) eds. F. P. Esposito and L. Witten.

[13] R. K. Sachs, *J. Math. Phys.* **3**, 908 (1962).

[14] S. A. Hayward, *Class. Quantum Grav.* **10**, 773 (1993).

[15] S. A. Hayward, *Class. Quantum Grav.* **10**, 779 (1993).

[16] H. Zum Hagen and H Seifert, G.R.G, **V8 N4**, 259 (1977).

[17] H. Friedrich, Proc. Roy. Soc. Lond. **A375**, 169 (1981).

[18] H. Friedrich, Proc. Roy. Soc. Lond. **A378**, 401 (1981).

[19] L. Tamburino and J. Winicour, *Phys. Rev.* **150**, 1039 (1966).

[20] N. T. Bishop, R. Gómez, L. Lehner, M. Maharaj and J. Winicour, *Phys. Rev. D*,**56** 6298 (1997).

[21] R. Gómez, L. Lehner, R. Marsa, and J. Winicour, *Phys. Rev. D* **57**, 4778 (1997).

[22] K. Thorne. in *Magic without Magic; John Archibald Wheeler*, ed. J. Klauder (Freeman, San Francisco, 1972) p. 231.

[23] R. K. Sachs, *Proc. Roy. Soc. London* **A264**, 309 (1961).

[24] L. P. Eisenhart, *An Introduction to Differential Geometry* (Princeton UP, Princeton, 1940), p. 272.

[25] L. Smarr, *Phys. Rev.* **D7**, 289 (1973).

[26] J. Massó, E. Seidel. W-M Suen and P. Walker, "Event Horizons in Numerical Relativity II: Analyzing the Horizon", gr-qc/9804059.

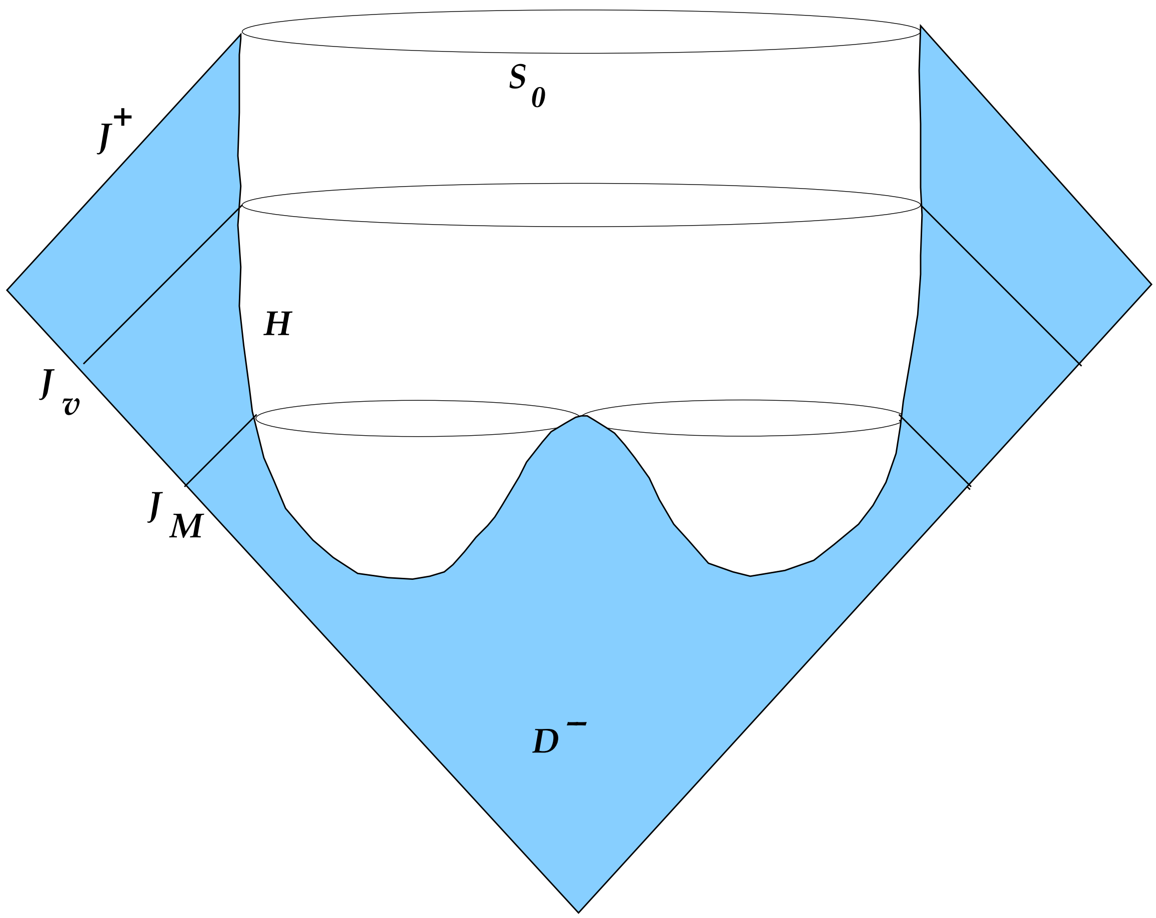

FIG. 1. A portion of the space-time prior to the coalescence of two black holes. The parameter v labels the advanced time on a family of incoming null hypersurfaces. D^{-} is the domain of dependence of characteristic data given on the event horizon $\mathcal{H}$ and on J^{+}.

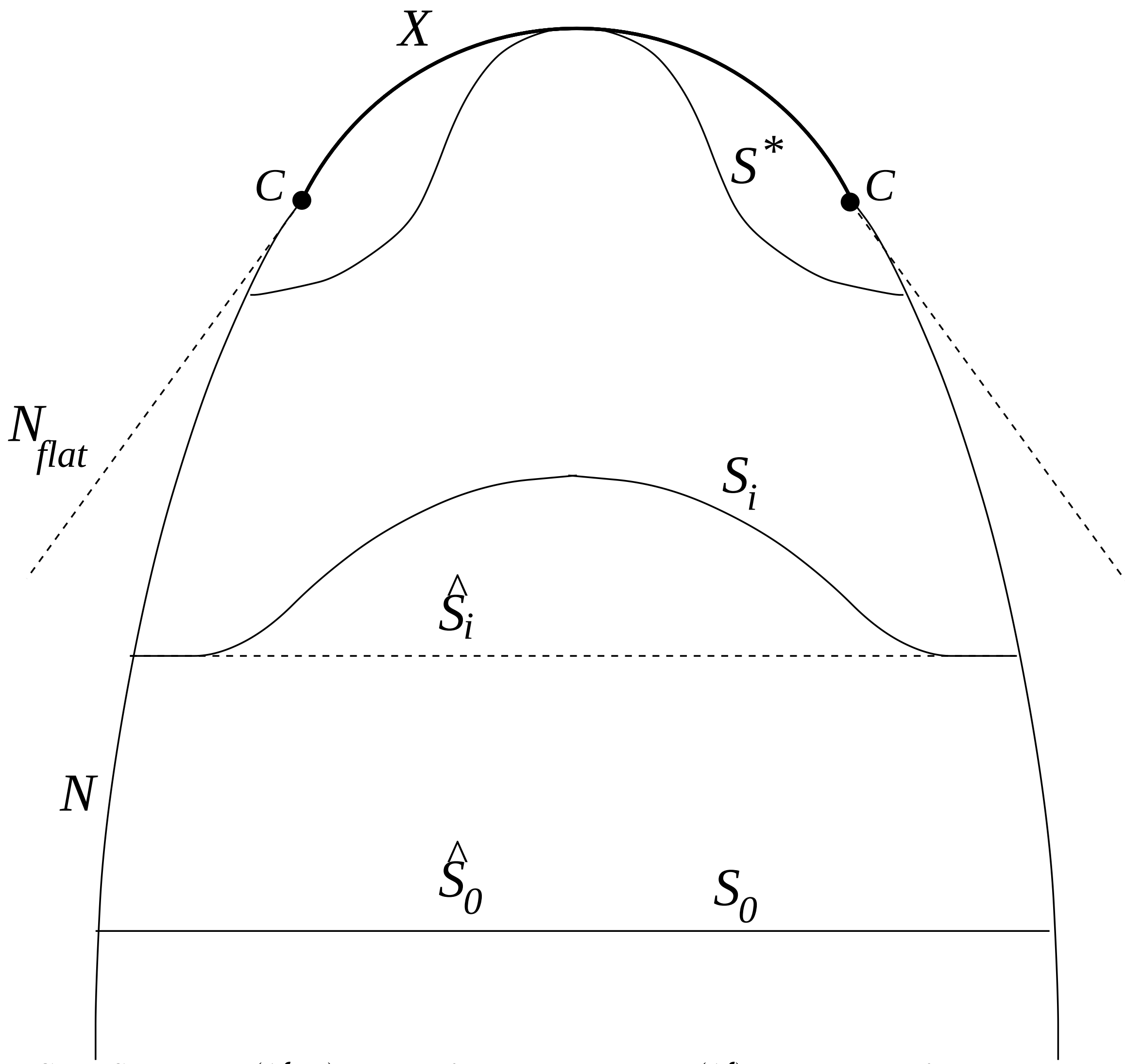

FIG. 2. Spheroidal ($\mathcal{N}_{flat}$) and conformally spheroidal ($\mathcal{N}$) null hypersurfaces: Factoring out the rotational symmetry allows the foliations to be depicted as lines from pole to pole. The Minkowski foliation indicated by $\hat{S}_i$ is drawn horizontally. The curved affine foliation is indicated by S_i.

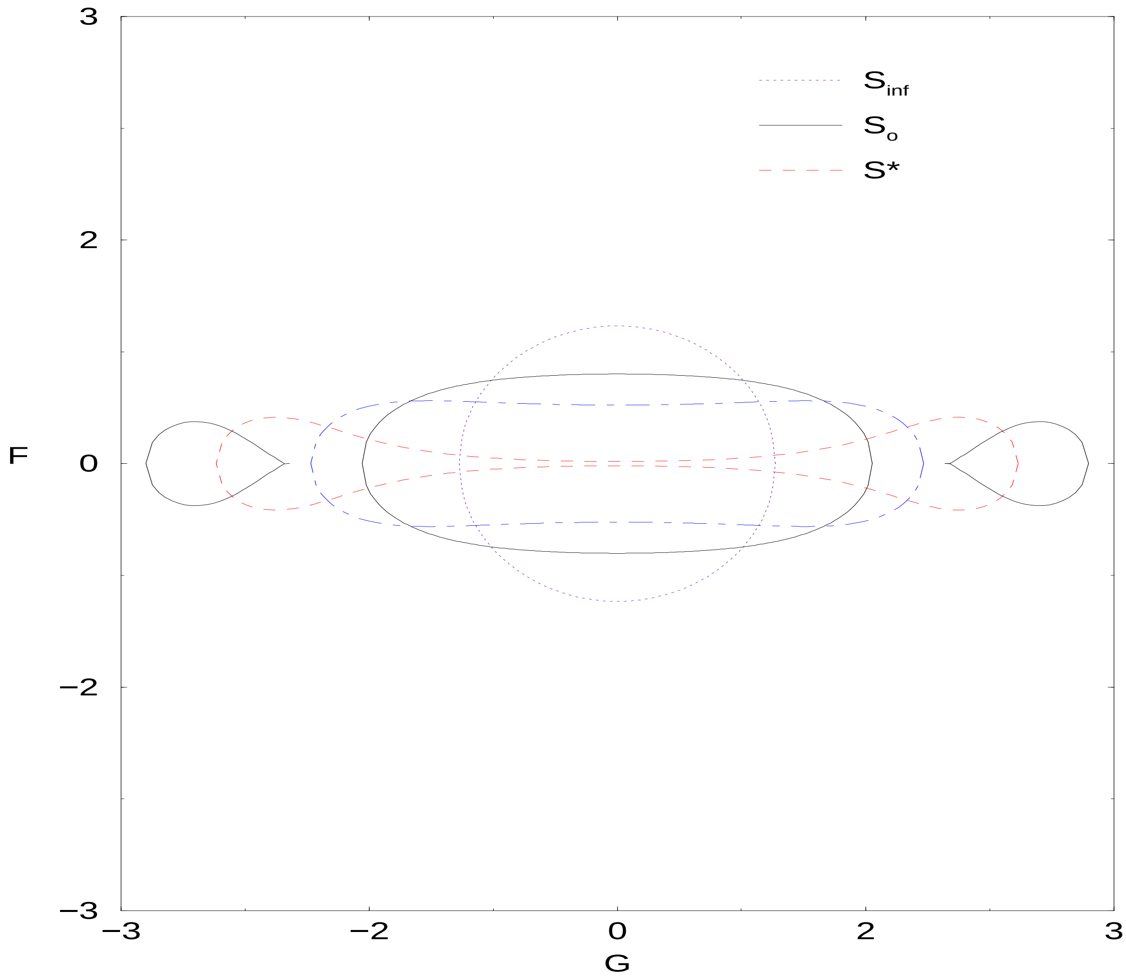

FIG. 3. Embedding snapshots profiling fission of an initially spheroidal white hole $\mathcal{S}_0$ in terms of the coordinates F and G: The white holes are the surfaces formed by rotating the profiles about the horizontal G axis.

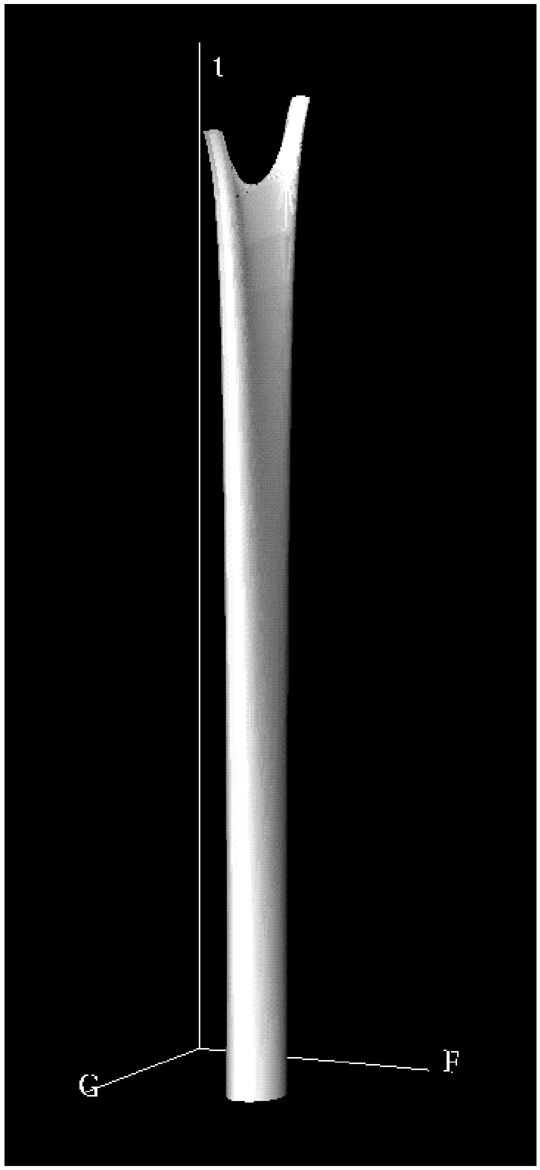

FIG. 4. The embedding history of the axisymmetric fission of a white hole into two white holes: The time slices S_t are horizontal and proceed upward as t increases.. The spatial origin of the embedding axes is offset from the center for clarity. The suppressed symmetry dimension corresponds to a rotation about the G axis. The history extends into both the future and past of the initial surface $\mathcal{S}_0$, which lies approximately halfway up the picture. A time reversed view gives the pair-of-pants picture for the head on collision of two black holes.

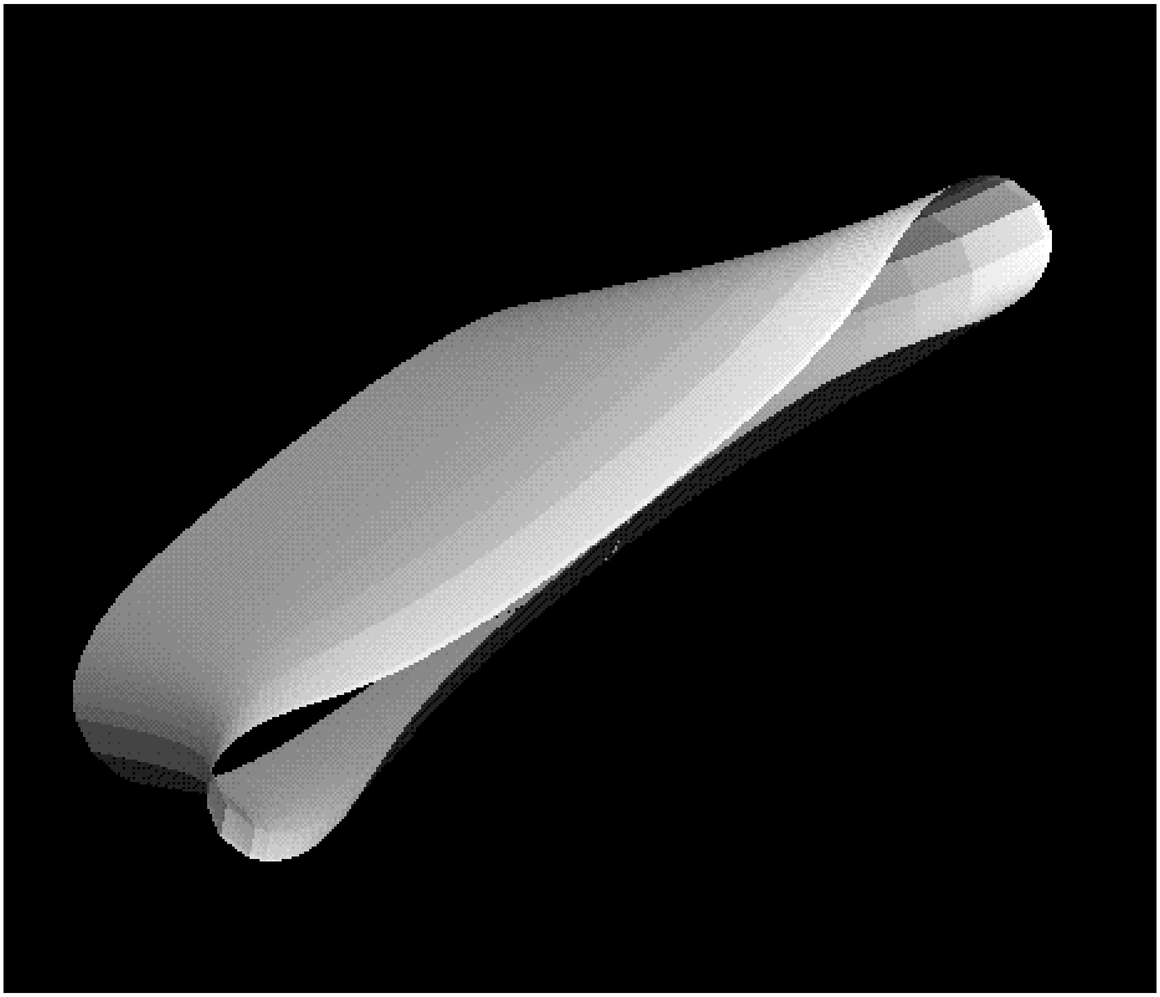

FIG. 5. A downward view of the portion of the embedding history from $\mathcal{S}_0$ up to the verge of bifurcation where the light rays at opposite points on the equator are about to cross.

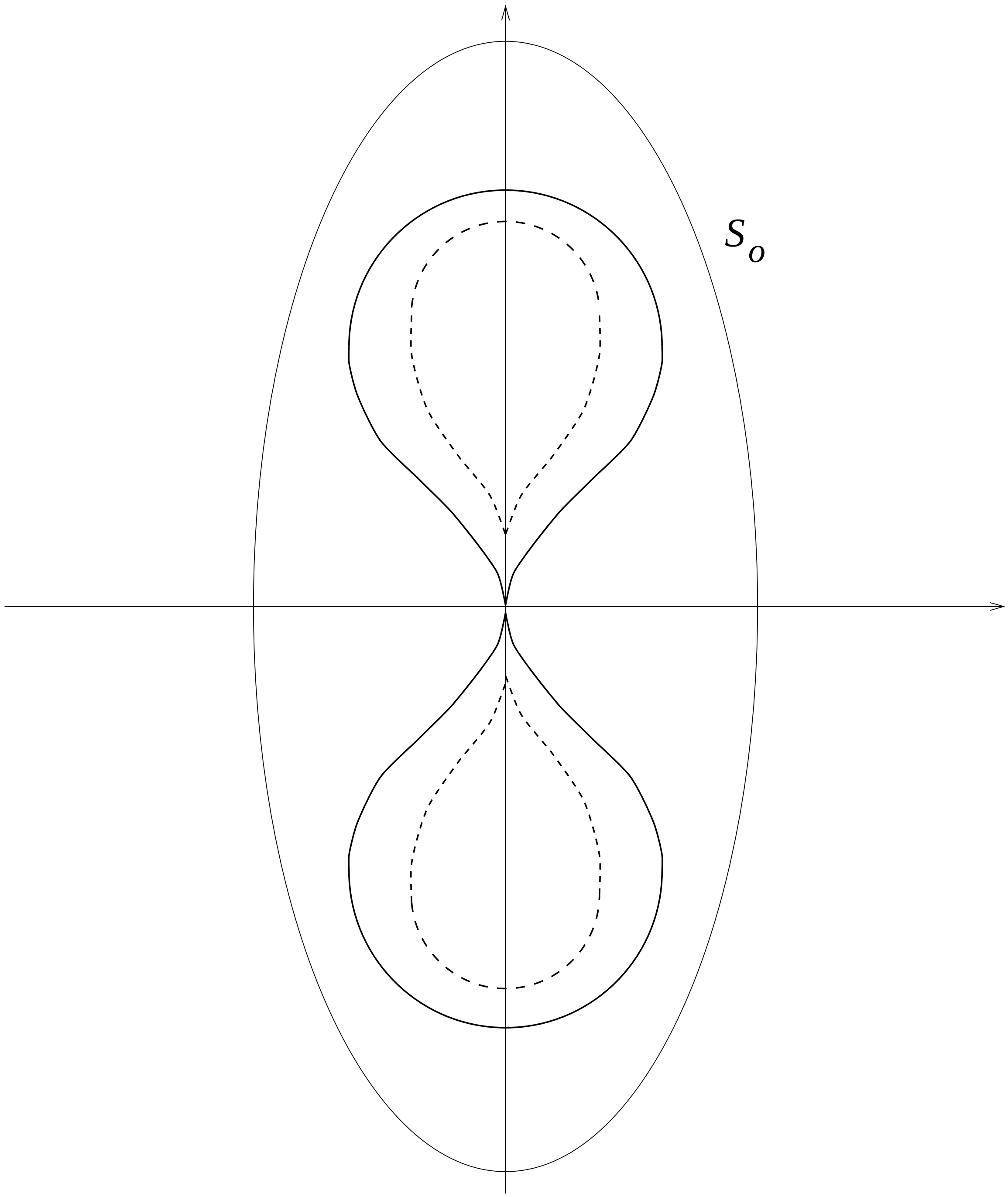

FIG. 6. Schematic profiles of an initially spheroidal white hole S_0 going through a toroidal stage. The rotation axis is vertical. The heavy solid line depicts the shape just prior to formation of the torus. The inner rim of the torus (dashed line) has a non smooth edge.